How does clamping pressure influence actuation performance of soft ionic polymer–metal composites?

2013 Smart Mater. Struct. 22 025014

(http://iopscience.iop.org/0964-1726/22/2/025014)

Smart Mater. Struct. **22** (2013) 025014 (11pp) doi:10.1088/0964-1726/22/2/025014

How does clamping pressure influence actuation performance of soft ionic polymer–metal composites?

Hossein Moeinkhah[1,2], Jin-Young Jung[1], Jin-Han Jeon[1], Ali Akbarzadeh[2], Jalil Rezaeepazhand[2], K C Park[1,3] and Il-Kwon Oh[1]

[1] Division of Ocean Systems Engineering, School of Mechanical, Aerospace and Systems Engineering, Korea Advanced Institute of Science and Technology, 335 Gwahak-ro, Yuseong-gu, Daejeon 305-701, Republic of Korea
[2] Department of Mechanical Engineering, Ferdowsi University of Mashhad, PO Box: 9177948944-11, Iran
[3] Department of Aerospace Engineering Sciences, University of Colorado at Boulder, Campus Box 429 Boulder, CO 80309-0429, USA

E-mail: ikoh@kaist.ac.kr

Received 14 September 2012, in final form 3 December 2012
Published 9 January 2013
Online at stacks.iop.org/SMS/22/025014

Abstract
The effect of clamping pressure on the actuation performance of ionic polymer–metal composite (IPMC) actuators is newly investigated by carefully considering changes of mechanical stiffness and electrical resistance due to the interfacial contacts between the IPMC and clamping devices. During the clamping process, the soft ionic exchangeable polymer membrane will be squeezed along the thickness direction in the clamping area, resulting in a change of the mechanical stiffness of the cantilevered IPMCs. Also, the electrical contact resistance between two electrodes of the IPMC and the clamping device will be greatly changed according to the change of clamping pressures. Present experimental results show that clamping pressures between the IPMC and the clamping device will strongly affect the actuation performance of the IPMC actuators. An exact electro-mechanical model is developed to fully describe dynamics of the IPMC actuators by considering structural damping, hydrodynamic loading and electro-mechanical force. This study shows that there exists an optimal clamping pressure to obtain the largest bending deformation of the IPMC actuator because of a trade-off between mechanical stiffness and electrical contact resistance.

(Some figures may appear in colour only in the online journal)

1. Introduction

To date, electro-active polymers (EAPs) have been intensively studied because of their huge potential applications in robotics, biomedical devices and artificial muscles. The ionic polymer–metal composite actuators are considered as a class of EAPs which may be an excellent candidate for biomimetic sensors and actuators [1]. The IPMC actuator shows a large bending deformation under a very low input voltage and current due to the migration of cations with water molecules inside the ion exchangeable polymer membranes. The IPMC actuators [2–4] have several advantages, such as low driving voltage or current, large strain, biomimetic activation and low power consumption. Therefore, the IPMC actuators have many potential applications in biomimetic robots [5–7, 38–40], industrial and biomedical devices [8], and space-effective manipulators [9–12].

The IPMC actuator is composed of a soft ionic polymer membrane and two thin metallic electrode layers. To activate the IPMC actuator, an external clamping device with electrical wires should be integrated with top and bottom electrodes of the IPMC actuators. The external clamping pressure

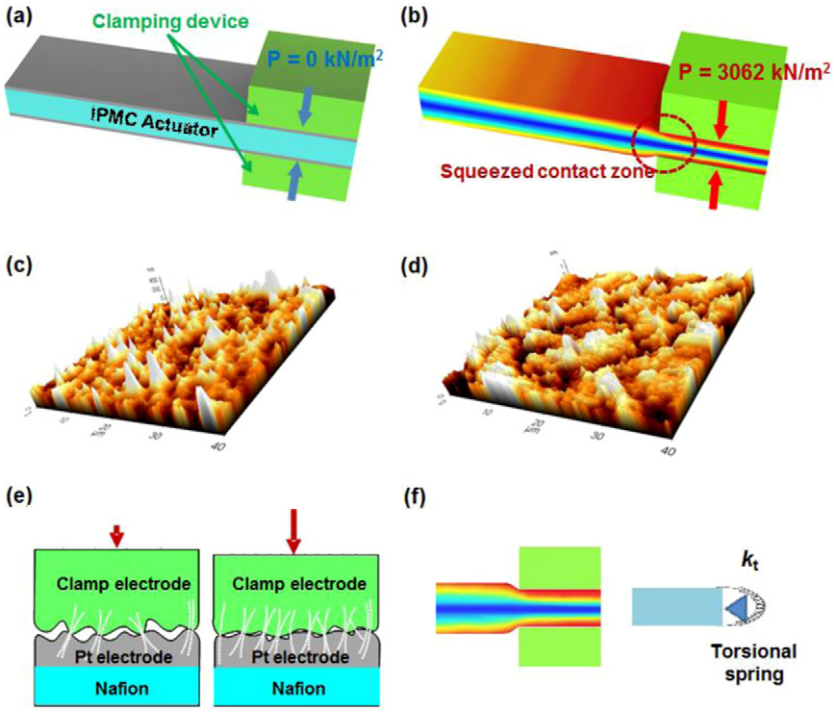

Figure 1. Clamped boundary conditions of cantilevered IPMC actuators. (a) Initial configuration before clamping, (b) deformation under clamping pressure, (c) AFM image of surface electrode of clamping device, (d) AFM image of platinum electrode in IPMC actuator, (e) electrical effect of clamping pressure (current flows under low and high clamping pressures) and (f) mechanical effect of clamping pressure (stiffness changes).

applied to both noble metallic electrodes will make the soft ionic polymeric layer mechanically deformed and squeezed. Figure 1(a) shows the initial configuration of an IPMC actuator before starting the clamping process and figure 1(b) shows the deformed shape of the soft IPMC actuator in the clamping area when the clamping pressure is applied. Under very small clamping pressures, the deformation during the clamping process is initially elastic and mechanical stiffness will be increased due to much tighter boundary conditions. However, by increasing the clamping pressure over the optimum level, the softer material deforms drastically, resulting in a reduction of the mechanical stiffness and porosity of the polymeric membrane and an increase of the electrical input power required to activate the IPMC actuator. Furthermore, a large clamping pressure may create electrical shorts and mechanical damage inside the actuator [13, 14]. All of these factors can cause a strong decrease or increase of the actuation performance of the IPMC under a certain clamping pressure. However, to our best knowledge, the mechanical and electrical effects of the clamping pressure on the actuation performance of IPMC actuators have not been investigated until now.

The morphology of the two electrodes in the contact surfaces of the clamping devices plays a significant role in the mechanical and electrical responses of an IPMC actuator. Figures 1(c) and (d) present real atomic force microscope (AFM) images obtained from the electrode surfaces of the IPMC and the clamping device, respectively. The AFM image highlights the considerably anisotropic nature of the surface, with high ridges and deep valleys. Based on the contact mechanics [13], when two surfaces contact each other with a very small compressive force, the roughness features of the contacting surfaces decrease the actual contact area and current flows only through the contact asperities, which results in a voltage drop across the interface. A schematic diagram of real contact spots and the current flow are shown in figure 1(e). Under low clamping pressure, the small interfacial contact area will cause very loose clamping boundary conditions and may increase the contact resistance between the two electrodes of the IPMC and the clamping device. The actuation performance of the IPMC actuator under the very low clamping pressure will not be good as reported in the fuel cell study [14].

The roughness of the two contact surfaces not only influences the current flow and voltage drop in the actuator, but also affects the mechanical stiffness of the actuator itself. During the clamping process, the soft polymeric membrane in the boundary area of the clamping device will be deformed because of its low elastic modulus. Moreover, the roughness of the contact surface, as shown in figure 1(f), leads to a non-uniform distribution of clamping pressure in this area. For modeling this non-uniform force distribution, we will model the clamping boundary condition with a torsional spring. It was found that the clamping pressure influences the performance of the polymer electrolyte membrane fuel cell by changing the contact resistance and material properties [15–17]. But in the case of soft actuators, up to now, there is no report estimating the effect of clamping pressure on actuation performance. Thus, it is essential to investigate

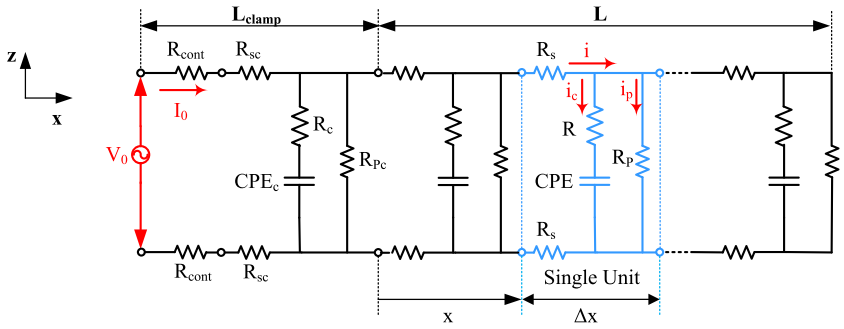

Figure 2. Distributed *RC* model of an IPMC actuator considering the clamping area.

the mechanical and electrical contact behavior between the clamping device and the IPMC actuator.

In this paper, we first investigate the effect of clamping pressure on the actuation performance of IPMC actuators experimentally and analytically. Present results show that there is an optimal clamping pressure for obtaining the best performance of an IPMC actuator in underwater conditions. To carefully explain the highly nonlinear dynamic responses of IPMC actuators under different clamping conditions, we develop a complete analytical dynamic model incorporating the effects of electrical and mechanical contacts. The electro-mechanical dynamic model consists of an electrical impedance model based on a distributed resistance–capacitance (*RC*) line with constant phase elements, and the mechanical dynamic model is carefully derived by considering structural damping and hydrodynamic loading effects. This proposed analytical model shows good agreements with experimental results.

2. Electro-mechanical model

For practical applications of the IPMC actuators, it is essential to understand their dynamic behaviors. Several dynamic models have been proposed for predicting the behavior and performance of IPMC actuators. They may be classified into three categories, namely the black box model [18], gray box model [19, 20] and physical model [21–25, 41, 42]. Chen *et al* [26] reported the modeling of a robotic fish propelled by an IPMC actuator by considering the interactions between IPMC and fluid. A finite element method was proposed by Yim *et al* [27] for modeling the motion of an IPMC actuator under water. They used an empirical *RC* circuit to predict the bending moment of an IPMC under electrical stimuli. Capacitance formed between two electrodes and internal resistance of the ionomeric polymer can be modeled as a simple *RC* circuit. There are many reports in the literature about IPMC modeling based on an equivalent electrical circuit where the voltage is correlated to the tip displacement by coupling electrical and mechanical parameters [28–31, 37]. One of the key factors that cause energy loss in the actuator is the resistance elements of the equivalent electrical circuit, which influences the performance of the actuator. Among several resistance elements, the electrical contact resistance between the IPMC electrodes and clamping device significantly influences the actuation performance of an IPMC.

The electrical model is related to the input voltage and ion movement inside the IPMC actuator, while the electro-mechanical model describes the relation between input voltage and bending displacement of the actuator. It is well known that the process can be modeled based on an electrical circuit [18, 19]. Bao *et al* [32] represented that the lumped *RC* model could not fit the time response between the experimental and simulated data for an IPMC sample. The dendrite structure of electrodes causes variation in the capacitance values in the IPMC model. This effect was incorporated in the distributed model of the IPMC.

The resulting distributed *RC* model can be described by a series of similar circuits with discrete elements that are coupled with a lumped electrical circuit, for clamping area, as illustrated in figure 2. According to the figure, we have represented the ion movement with a series of *RC* transition lines. By modeling an electro-mechanical behavior of an IPMC with an ideal capacitor, there is an assumption that the surface under investigation is homogeneous, which is normally not the case. Thus the lack of homogeneity is modeled with a constant phase element (CPE, [43]). A constant phase element is an equivalent electrical circuit component that models the behavior of a double layer, which is an imperfect capacitor. The CPE impedance, Z_{CPE}, is expressed in terms of the CPE index n and Q_0 as

$$Z_{\mathrm{CPE}} = \frac{1}{Q_0 s^n} \tag{1}$$

where $Q_0 = 1/|Z|$ at $\omega = 1$ rad s^{-1}. The CPE index n ranges from 0 to 1. When $n = 1$, Z_{CPE} is identical to the capacitor impedance and n means the deviation from the ideal capacitive impedance. In this model, R_{cont} and R_{s} are the contact resistance and the surface resistance of the IPMC, respectively. The branch CPE-R represents the electrical behavior at the interface of the metal and polymer. The electrolyte between the electrodes introduces an internal resistance, which is represented by R_{p} as a shunt resistor between two electrodes in a single unit. The subscript c shown in figure 2 means the lumped model parameters defined in the clamping area.

2.1. Derivation of electrical impedance model

As the first step in deriving the actuation model of an IPMC actuator, we develop the electrical impedance model. By applying Kirchhoff's law to the infinitesimal element, Δx, shown in figure 2, the following current and voltage relations can be written in the Laplace domain:

$$\frac{\partial i(x,s)}{\partial x} = -(i_c(x,s) + i_p(x,s)) \tag{2}$$

$$\frac{\partial v(x,s)}{\partial x} = -2R_s i(x,s) \tag{3}$$

where

$$\begin{aligned} v(x,s) &= R_p i_p(x,s) = v_{CPE}(x,s) + R i_c(x,s) \\ i_c(x,s) &= Q_0 s^n v_{CPE}(x,s). \end{aligned} \tag{4}$$

Here, voltage, $v(x,s)$, and current, $i(x,s)$, are assumed to be functions of the distance along the x coordinate and Laplace domain s. $i_c(x,s)$ is the distributed current per unit length flowing through the ionic polymer due to the ion movement, $i_p(x,s)$ indicates the leaking current per unit length, and $i(x,s)$ is the surface current on the electrodes. Considering the lumped model in the clamping area as shown in figure 2, the equivalent circuit, which consists of two impedances $Z_1(s)$ (series) and $Z_2(s)$ (parallel), can be simply used as shown in figure 3. The two impedances can be expressed in the following form.

$$\begin{aligned} Z_1(s) &= 2(R_{cont} + R_{sc}) \\ Z_2(s) &= \frac{R_{Pc}(1 + R_c Q_{0c} s^{n_c})}{1 + (R_{Pc} + R_c) Q_{0c} s^{n_c}}. \end{aligned} \tag{5}$$

According to figure 3 and equation (5), the boundary conditions of voltage and current for the infinitesimal element are given by

$$\begin{aligned} v(0,s) &= V_0(s) - Z_1(s) I_0(s) \\ i(0,s) = I_0(s) - \frac{V_0(s) - Z_1(s) I_0(s)}{Z_2(s)}, &\qquad i(L,s) = 0. \end{aligned} \tag{6}$$

From equations (3), (4) and (6) the following voltage at x can be obtained:

$$\begin{aligned} v_{CPE}(x,s) &= V_0(s) - Z_1(s) I_0(s) \\ &\quad - 2\int_0^x R_s i(x,s)\,dx - R i_c(x,s). \end{aligned} \tag{7}$$

Using equations (4) and (7), the following relations for leaking and distributed current at x can be expressed as

$$\begin{aligned} i_p(x,s) &= \frac{1}{R_p}\left[V_0(s) - Z_1(s) I_0(s) - 2\int_0^x R_s i(x,s)\,dx\right] \\ i_c(x,s) &= \Theta(s)\left[V_0(s) - Z_1(s) I_0(s) - 2\int_0^x R_s i(x,s)\,dx\right] \end{aligned} \tag{8}$$

where

$$\Theta(s) = \frac{Q_0 s^n}{1 + R Q_0 s^n}. \tag{9}$$

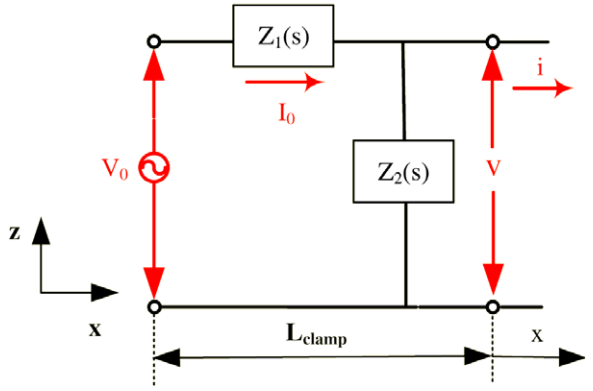

Figure 3. Equivalent circuit for lumped model in clamping area.

By substituting equation (8) into (2) the following relations are obtained:

$$-\frac{\partial i(x,s)}{\partial x} = M(s)V_0(s) - K(s)I_0(s) - N(s)\int_0^x i(x,s)\,dx \tag{10}$$

where $M(s) = \Theta(s) + \frac{1}{R_p}$, $K(s) = Z_1(s)M(s)$ and $N(s) = 2R_s M(s)$.

Equation (10) is an integro-differential equation for $i(x,s)$. After solving this equation, the surface current $i(x,s)$ is obtained:

$$\begin{aligned} i(x,s) &= i(0,s)\cosh(\sqrt{N(s)}x) - \frac{M(s)V_0(s)}{\sqrt{N(s)}}\sinh \\ &\quad \times (\sqrt{N(s)}x) + \frac{K(s)I_0(s)}{\sqrt{N(s)}}\sinh(\sqrt{N(s)}x). \end{aligned} \tag{11}$$

From the open ended boundary condition ($i(L,s) = 0$) and equation (6), the total actuation current $I_0(s)$ can be obtained. Therefore, the transfer function for impedance is concluded to be

$$\begin{aligned} Z(s) &= \frac{V_0(s)}{I_0(s)} = Z_1(s) \\ &\quad + \left(\frac{1}{Z_2(s)} + \frac{M(s)}{\sqrt{N(s)}}\tanh(\sqrt{N(s)}L)\right)^{-1}. \end{aligned} \tag{12}$$

Based on the physical parameters (see table 1 in section 4.1), and since $Z_2(s)$ includes the bulk resistance of the membrane, $Z_2(s) \gg 10^4$, which allows one to make an approximation for impedance, equation (12), in the low frequency range (<100 Hz)

$$Z(s) = \frac{V_0(s)}{I_0(s)} \simeq Z_1(s) + \frac{\sqrt{N(s)}}{M(s)\tanh(\sqrt{N(s)}L)}. \tag{13}$$

Therefore, from the above equations, the following relation for voltage and current can be obtained along the length of the actuator:

Table 1. Identified parameters of impedance model in the clamping area.

Parameters	Clamping pressure (kN m^{-2})	R_{cont} (mΩ cm^2)	R_{sc} (Ω cm^{-1})	R_c (Ω cm)	R_{Pc} (Ω cm)	Q_{0c}	n_c
Identified value	612	54.1281	22.53	7.5	2.529×10^4	0.0021	0.58
	1837	43.12	22.53	11.26	3.35×10^4	0.0015	0.64
	3062	38.75	22.53	14	3.83×10^4	0.0011	0.63
	4287	40.5	22.53	13.25	2.24×10^4	0.0012	0.65

$$\begin{aligned} v(x,s) &= V_0(s)\frac{\sqrt{N(s)}}{B(s)} \\ &\quad\times[\cosh(\sqrt{N(s)}x) - \tanh(\sqrt{N(s)}L)\sinh(\sqrt{N(s)}x)] \\ i(x,s) &= V_0(s)\frac{M(s)}{B(s)} \\ &\quad\times[\tanh(\sqrt{N(s)}L)\cosh(\sqrt{N(s)}x) - \sinh(\sqrt{N(s)}x)] \end{aligned} \tag{14}$$

where $B(s) = K(s)\tanh(\sqrt{N(s)}L) + \sqrt{N(s)}$.

2.2. Expression for ionic charge density in the polymer

Nemat-Nasser *et al* [24] assumed that the induced stress is proportional to the charge density

$$\sigma(x,s) = \alpha\rho(x,s) \tag{15}$$

where α is the coupling constant and $\rho(x,s)$ is the charge density. Thus, in the first step in calculating the induced stress, it is important to find an expression for the charge density through the length of the polymer. The ionic charge $\rho(x,s)$ is the total ionic current that passes through the polymer and density of charge; it is found by dividing the charge by the volume in each single unit. Then the ionic charge is expressed as

$$\rho(x,t) = \frac{Q(x,t)}{Wh\,\mathrm{d}x} = \frac{1}{Wh}\int\frac{i(x,t) - i(x+\mathrm{d}x,t)}{\mathrm{d}x}\,\mathrm{d}t \tag{16}$$

where W and h are the width and thickness of the actuator, respectively. This can be transformed into the Laplace domain

$$\begin{aligned} \rho(x,s) &= \frac{1}{Whs}\left(-\frac{\partial i(x,s)}{\partial x}\right) \\ &= \frac{1}{Wh}\frac{M(s)\sqrt{N(s)}}{sB(s)}V_0(s)g(x,s) \\ g(x,s) &= \cosh(\sqrt{N(s)}x) - \tanh(\sqrt{N(s)}L)\sinh(\sqrt{N(s)}x). \end{aligned} \tag{17}$$

This expression shows the charge density distribution along the length of the strip as a function of frequency.

2.3. Electro-mechanical model of IPMC

In order to obtain the dynamic equations of the flexible IPMC beam, Hamilton's variational principle was used. Based on Euler–Bernoulli beam theory, the following classical fourth-order PDE can be obtained by substituting the strain energy, kinetic energy, and virtual work into Hamilton's principle.

$$\begin{aligned} &\frac{\partial^2}{\partial x^2}\left(EI\frac{\partial^2 w(x,t)}{\partial x^2}\right) + \rho A\frac{\partial^2 w(x,t)}{\partial t^2} \\ &= F(x,t) = f_{app}(x,t) - f_{fluid}(x,t) \end{aligned} \tag{18}$$

where $w(x,t)$ is transverse displacement, I is the area moment of inertia, ρ is the density, E is the static Young's modulus which is obtained experimentally, A is the cross sectional area of IPMC and $F(x,t)$ is the distributed force density along the length of the actuator. The distributed force on the beam consists of two components; the applied force due to the actuation of the IPMC and the viscous fluid damping force from the water. The frequency response of an elastic beam is highly sensitive to the nature of the fluid in which it is immersed. In order to accurately predict the frequency spectrum, we must take into account the physical properties of the beam, as well as the surrounding fluid.

The viscous fluid damping force per unit length on a beam oscillating at a frequency ω (rad s^{-1}) can be expressed as [33, 44]

$$\begin{aligned} f_{fluid}(x,t) &= m_a(\omega)\frac{\partial^2 w(x,t)}{\partial t^2} + c_\nu(\omega)\frac{\partial w(x,t)}{\partial t} \\ m_a(\omega) &= m_d\,\mathrm{Re}(\Gamma_{rect}(\omega)), \\ c_\nu(\omega) &= -m_d\omega\,\mathrm{Im}(\Gamma_{rect}(\omega)) \end{aligned} \tag{19}$$

with

$$m_d = \rho_f(\pi/4)W^2 \tag{20}$$

where W is the width of the IPMC beam, ρ_f is the density of fluid, and $\Gamma_{rect}(\omega)$ is the hydrodynamic function. The quantity $m_a(\omega)$ is the added mass and $c_\nu(\omega)$ is the damping coefficient of the viscous fluid. The hydrodynamic function $\Gamma_{rect}(\omega)$ is obtained from the expression of the corresponding function for a circular cross section as [33, 44]

$$\Gamma_{rect}(\omega) = \Lambda_{corr}(\omega)\left(1 + \frac{4jK_1(-j\sqrt{jR_e})}{\sqrt{jR_e}K_0(-j\sqrt{jR_e})}\right) \tag{21}$$

where K_0 and K_1 are modified Bessel functions of the third type, $\Lambda_{corr}(\omega)$ is a complex valued correction function that corrects the results for a beam of circular cross section to a beam of rectangular cross section and

$$R_e = \frac{\rho_f\omega W^2}{4\mu_f} \tag{22}$$

is the Reynolds number. Strictly speaking, the hydrodynamic model is valid for a beam with infinite length.

Unlike the linear elastic materials, Nafion® typically exhibits viscoelastic behavior, in which the stress–strain relationship has both liquid-like and solid-like features. If linear viscoelastic behavior is assumed, the stress in the polymer is linearly related to both the strain and the strain

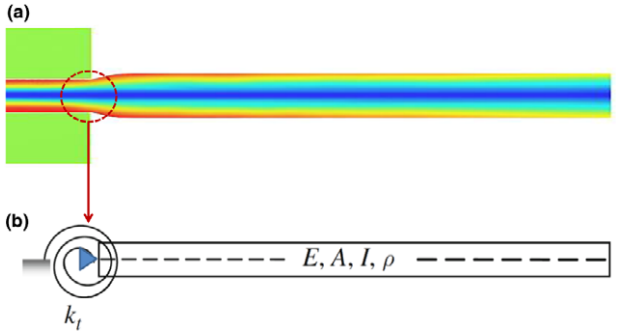

Figure 4. Boundary conditions of clamped IPMC actuator: (a) squeezed contact zone in the clamping area and (b) clamped boundary condition with torsional spring.

rate as

$$\sigma_x = E\left(\varepsilon_x + \frac{\gamma}{\omega}\frac{\partial \varepsilon_x}{\partial t}\right) \tag{23}$$

where γ is an empirically determined value. From the displacement field theory, it is seen that E can be replaced by $E(1+\frac{\gamma}{\omega}\frac{\partial}{\partial t})$. With equations (19) and (23), the beam dynamic equation (18) can be written as

$$\frac{\partial^2}{\partial x^2}\left(EI\left(1+\frac{\gamma}{\omega}\frac{\partial}{\partial t}\right)\frac{\partial^2 w(x,t)}{\partial x^2}\right) + c_v(\omega)\frac{\partial w(x,t)}{\partial t} + \mu_v(\omega)\frac{\partial^2 w(x,t)}{\partial t^2} = f_{\text{app}}(x,t) \tag{24}$$

where $\mu_v(\omega) = \rho A + m_a(\omega)$ indicates the summation of structural inertia and fluidic added mass terms defined in equations (18) and (19). Equation (19) is the non-homogeneous partial differential equation incorporating the effect of contact resistance in the right-hand side. When considering the distributed electrical model, from equations (15) and (17) we can obtain the actuation induced bending moment

$$M_{\text{app}} = 2\int_0^h z\sigma W\,\mathrm{d}z = 2W\int_0^h \alpha\rho(x,s)z\,\mathrm{d}z = \alpha h\frac{M(s)\sqrt{N(s)}}{sB(s)}V_0(s)g(x,s). \tag{25}$$

Then the distributed force along the length in the Laplace domain will be obtained as

$$f_{\text{app}}(x,s) = \frac{\partial^2 M_{\text{app}}(x,s)}{\partial x^2}. \tag{26}$$

During the clamping process, the boundary of the IPMC actuator in the clamping area is deformed along the thickness direction because of its low elastic modulus. Moreover, the roughness of the contact surface, as shown in figure 1, leads to non-uniform distribution of clamping pressure in this area. Figure 4(a) shows a schematic diagram of the physical deformation when the compression force is applied. For modeling this effect, the clamping boundary is modeled with a torsional spring as shown in figure 4(b).

Based on this assumption, the boundary conditions for equation (24) are

$$EI\frac{\partial^2 w(0,t)}{\partial x^2} = k_t\frac{\partial w(0,t)}{\partial x}, \qquad w(0,t) = 0 \tag{27a}$$

$$\frac{\partial^2 w(L,t)}{\partial x^2} = \frac{\partial^3 w(L,t)}{\partial x^3} = 0. \tag{27b}$$

According to the mode superposition principle, we can discretize the partial differential equation (24) into a set of ordinary differential equations. The flexural deflection of the cantilever beam can be estimated approximately by using the assumed modes [34]

$$w(x,t) = \sum_{i=1}^{n}\varphi_i(x)q_i(t) \tag{28}$$

where φ_i is the normal mode corresponding to the natural frequency ω_i and q_i is the corresponding generalized coordinate. Using the separation of variables method, the following eigenfunctions are obtained:

$$\varphi_i(x) = \frac{\overline{K}_t}{2(\beta_i L)}(\cos(\beta_i x) - \cosh(\beta_i x))(1+\lambda_i) + \lambda_i\sin(\beta_i x) + \sinh(\beta_i x) \tag{29}$$

where β_i can be obtained based on the characteristic equation

$$(\beta_i L)(\cos(\beta_i L)\sinh(\beta_i L) - \sin(\beta_i L)\cosh(\beta_i L)) + \overline{K}_t(1+\cos(\beta_i L)\cosh(\beta_i L)) = 0. \tag{30}$$

Moreover

$$\lambda_i = \frac{1+\cos(\beta_i L)\cosh(\beta_i L)+\sin(\beta_i L)\sinh(\beta_i L)}{1+\cos(\beta_i L)\cosh(\beta_i L)-\sin(\beta_i L)\sinh(\beta_i L)}, \qquad \overline{K}_t = \frac{k_t}{EI/L}. \tag{31}$$

By applying orthogonal conditions of normal modes, the uncoupled ordinary differential equations for the generalized coordinates, $q_i(s)$, can be obtained as

$$q_i(s) = [s^2 + 2\xi_i\omega_i s + \omega_i^2]^{-1}f_i(s), \qquad i = 1,2,\ldots,n \tag{32}$$

where the natural frequency ω_i and the damping ratio ξ_i for the ith mode are

$$\omega_i = (\beta_i L)^2\sqrt{\frac{EI}{\mu_v(\omega_i)L^4}}, \qquad \xi_i = \frac{1}{2}\left(\gamma - \frac{m_d\,\mathrm{Im}(\Gamma_{\text{rect}}(\omega_i))}{\mu_v(\omega_i)}\right) \tag{33}$$

and

$$f_i(s) = \frac{1}{M_i}\int_0^L f_{\text{app}}(x,s)\varphi_i(x)\,\mathrm{d}x = \Pi_i(s)U(s) \tag{34}$$

where M_i is

$$M_i = \int_0^L \mu_v(\omega_i)\,\varphi_i^2(x)\,\mathrm{d}x. \tag{35}$$

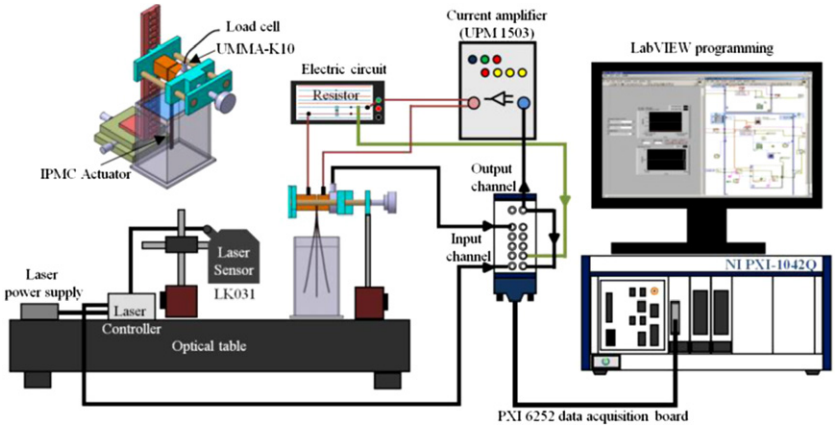

Figure 5. Experimental setup for measurement of clamping pressure and tip displacement of IPMC.

After integrating (34) over the domain, the result can be simplified as [26]

$$\Pi_i(s) = \frac{\alpha h M(s) N(s)}{s M_i}(1-b)[a_1 + b_1 - c_1 - d_1 - \lambda_i(a_1 - b_1 + jc_1 - jd_1)] \tag{36}$$

and

$$\begin{aligned} a_1 &= \frac{\sinh((a+\beta_i)L)}{a+\beta_i}, \\ b_1 &= \frac{\sinh((a-\beta_i)L)}{a-\beta_i}, \\ c_1 &= \frac{\sinh((a+j\beta_i)L)}{a+j\beta_i}, \\ d_1 &= \frac{\sinh((a-j\beta_i)L)}{a-j\beta_i}, \\ a &= \sqrt{N(s)}, \qquad b = \tanh(\sqrt{N(s)}). \end{aligned} \tag{37}$$

By substituting equations (29) and (32) into (28), the transfer function $H(s)$ can be obtained as

$$H(s) = \frac{w(L,s)}{V_0(s)} = \sum_{i=1}^{n} \varphi_i(L)[s^2 + 2\xi_i\omega_i s + \omega_i^2]^{-1}\Pi_i(s). \tag{38}$$

3. Experimental setup

An IPMC was fabricated from Nafion (N-117, DuPont) through an electroless plating process [35]. The dimensions of the specimen were about 30 mm × 4 mm × 0.22 mm. An impedance analyzer (VersaSTAT3-model 616A) was used for measuring the complex impedance of the IPMC. To measure the electro-mechanical responses of the actuator, a laser displacement sensor (Keyence, LK-031), a current amplifier (UPM1503) and an NI-PXI 8110 data acquisition system were used. The IPMC actuator was activated under distilled water as shown in figure 5, and the actuation current values were calculated by measuring the voltage across a resistor in series with the IPMC actuator. In order to investigate the effect of contact force on the performance of the IPMC actuator, various clamping pressures of 612 kN m^{-2}, 1837 kN m^{-2}, 3062 kN m^{-2} and 4287 kN m^{-2} (corresponding to clamping forces of 9.8 N, 29.4 N, 49 N and 68.6 N, respectively) were applied to the actuator in the present study. A load cell (Dacell model UMMA-K10) was integrated with the clamping device to measure the external load up to a maximum of 98 N and the clamped area was 4 mm × 4 mm. The overall integrated measurement system is shown in figure 5.

4. Results and discussion

4.1. Verification of contact resistance and optimum clamping pressure

In other to validate the values of contact resistance from the impedance model presented here, experimental results were captured from the impedance analyzer with different clamping pressures, P, as shown in figure 6(a). The nonlinear least square method was used to find the optimum parameter x^* that minimizes the squared error between the empirical impedance response, $\hat{z}_i (i = 1, 2, \ldots, n)$, and the theoretical model. The identified parameters of the impedance model for different clamping pressures are listed in table 1. The values of surface electrode resistance can be measured directly using a four probe system. The parameters in the distributed area are assumed to be the same as reported in table 1.

As discussed earlier, the surface roughness of the contacting objects influences the interfacial contact resistance. Under a low clamping pressure condition, the roughness features of the contacting surfaces decrease the actual contacting area and the interfacial contact resistance is increased. Experimental results show a good agreement with this phenomenon. As illustrated in figure 6(b), when the clamping pressure is increased up to 3062 kN m^{-2} the interfacial contact resistance is decreased, but above 3062 kN m^{-2} the contact resistance shows a reversal in behavior due to the deformation of materials. Since the IPMC is made of highly porous and soft materials, it may also be deformed greatly due to the lowest elastic modulus during the clamping process. At high clamping pressure, the porosity of the IPMC actuator, in the contacting region, can be changed. A higher porosity may be expected to decrease the contact area, thus the contacting resistance is increased. Also, when the clamping pressure is too high, the membrane and metallic

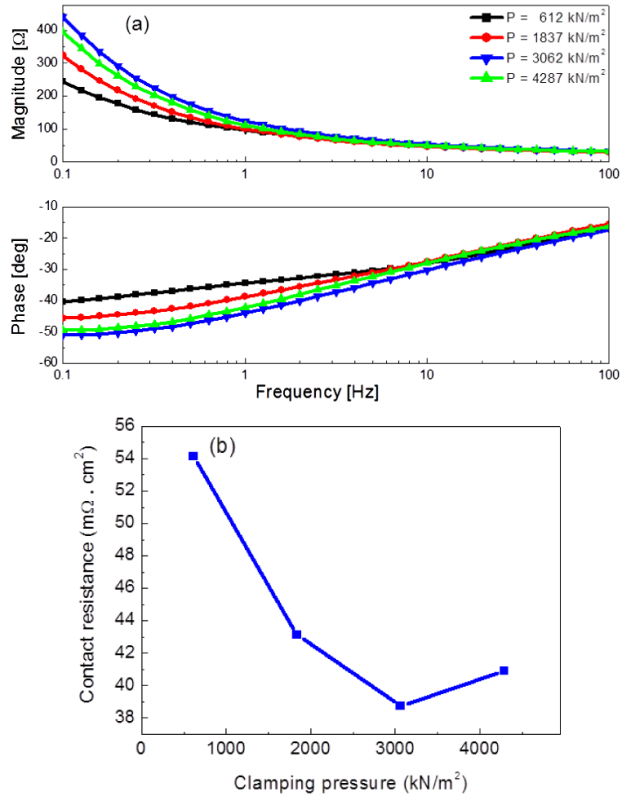

Figure 6. Impedance analyses: (a) comparison of experimental impedance responses at different clamping pressures and (b) variation of interfacial contact resistance over the clamping pressure range.

electrodes of the IPMC may be damaged, causing cell leakage, internal shorts and increase of contact resistance [36].

To investigate the performance of an IPMC actuator under different clamping pressures, the harmonic responses subject to the peak voltage of 1 V and frequency of 0.1 Hz and also step responses were examined. Figures 7 and 8 show step and harmonic responses of the IPMC actuator over the range of different clamping pressures. The present results show that 3062 kN m^{-2} is the optimum clamping pressure for getting the best performance from the IPMC actuators.

4.2. Verification of the actuation model

The frequency response functions (FRFs) based on small-oscillation theory were also measured through a swept-sine method by applying sinusoidal actuation signals $V(t)$ with amplitude 0.5 V and frequency from 0.1 to 20 Hz. Figure 9 shows the frequency response functions of the actuator under different clamping pressures. Present results indicate that the first natural frequency of the IPMC actuator is increased by increasing the clamping pressure up to the optimum level.

Based on the present results and equation (30), the non-dimensional constant of a torsional spring can be obtained for corresponding clamping pressures. Table 2 shows the variation of torsional spring constant during the clamping process.

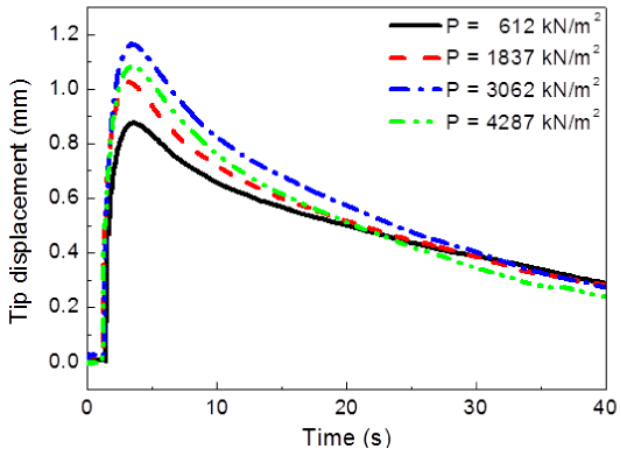

Figure 7. Comparison of step responses in different clamping pressures.

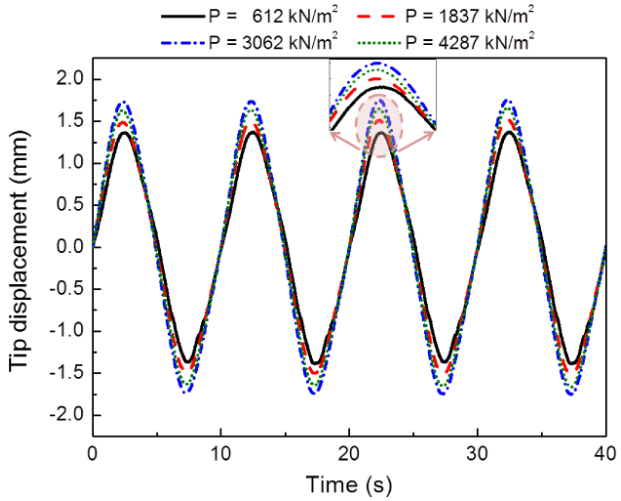

Figure 8. Comparison of harmonic responses in different clamping pressures.

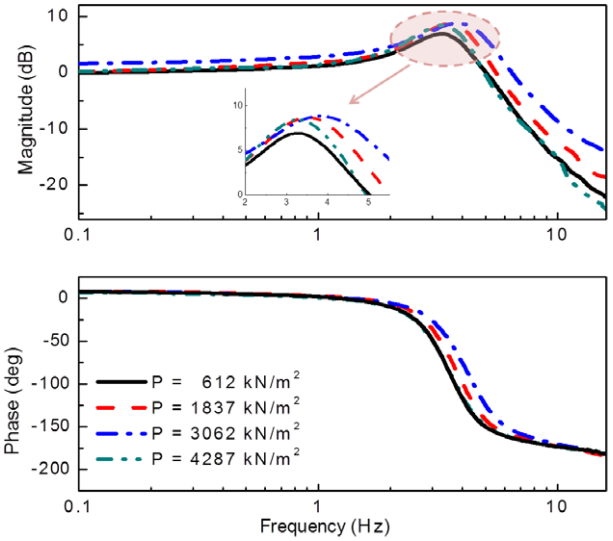

Figure 9. Experimental FRF responses of IPMC actuators under different clamping pressures.

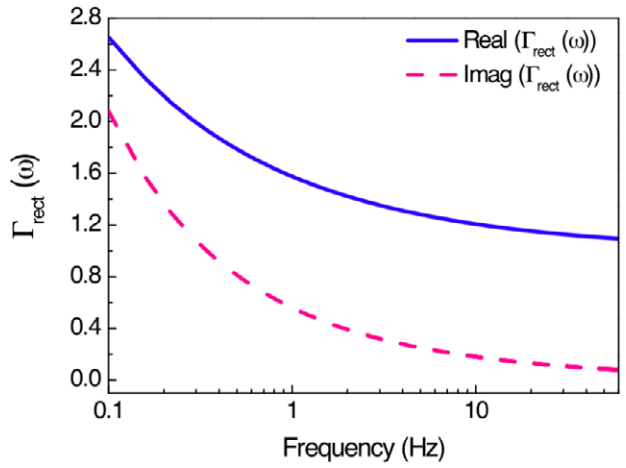

Figure 10. Hydrodynamic functions of IPMC actuator under water.

Table 2. Non-dimensional constant of torsional spring corresponding to clamping pressures.

	Clamping pressure (kN m^{-2}), P			
	612	1837	3062	4287
First natural frequency, ω_1	3.29	3.54	3.78	3.29
Non-dimensional torsional spring, $\overline{K}_t$	4.17	5.67	8.02	4.17

Table 3. Estimated values of remaining dynamic parameters.

E (MPa)	ξ_1	μ_υ (kg m^{-1})	γ	α (J C^{-1})
313	0.18	0.02	0.14	0.105

In other to validate the proposed dynamics model, we must obtain the dynamic parameters of the actuator. The first natural frequency and damping ratio are acquired from the passive vibration test of IPMC in water. Figure 10 shows the hydrodynamic function of the IPMC beam over a range of different frequencies based on equation (21). From this figure one can get $\mathrm{Re}(\Gamma_{\mathrm{rect}}(\omega_1)) = 1.32$ and $\mathrm{Im}(\Gamma_{\mathrm{rect}}(\omega_1)) = 0.2886$.

The Matlab function *lsqcurvefit*, which is usually used for nonlinear curve fitting, was used to find the remaining parameters, α and γ, that minimize the square error between the empirical frequency response function and $H(s)$. Table 3 shows all the parameters related to the beam dynamics.

In figure 11, we compared the frequency responses of our theoretical model with experimental results for two different clamping pressures of 612 and 3062 kN m^{-2}. The present analytical model can be used to predict the frequency response of the actuator for different clamping pressures. The time response of the actuator through the whole length, for the case of 612 kN m^{-2} and 3062 kN m^{-2}, is evaluated, as shown in figures 12 and 13 respectively. These plots correspond to an applied harmonic response subject to electrical input potential with peak voltage 1 V and frequency 0.1 Hz.

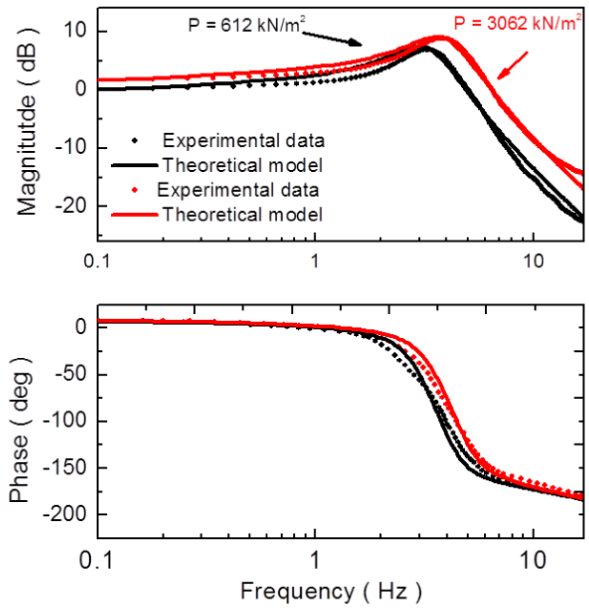

Figure 11. Comparison of proposed analytical frequency responses with experimental results.

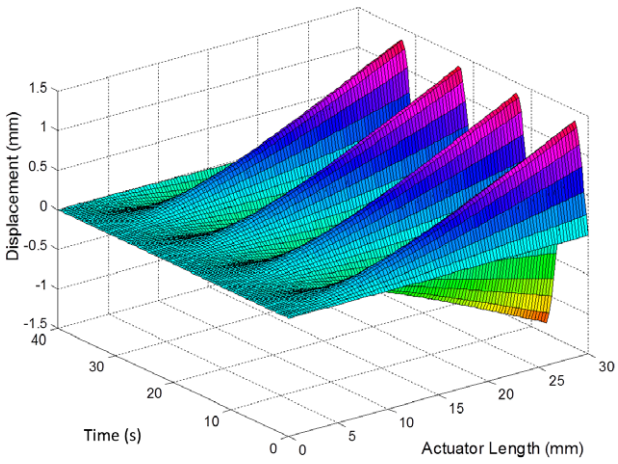

Figure 12. Estimated harmonic response of IPMC actuator subject to clamping pressure of 612 kN m^{-2}.

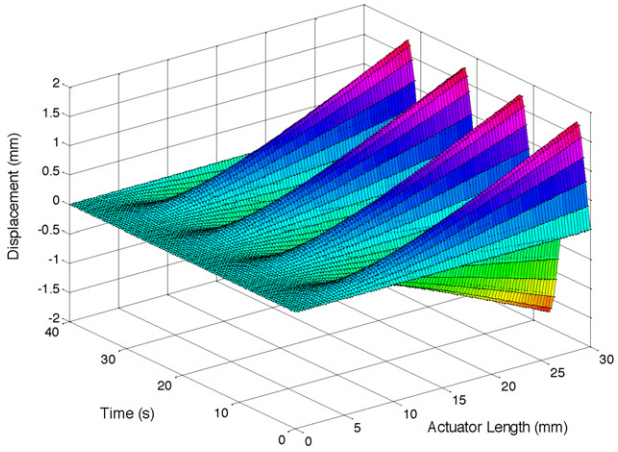

Figure 13. Estimated harmonic response of IPMC actuator subject to clamping pressure of 3062 kN m^{-2}.

5. Conclusion

The effect of the clamping pressure on the performance of an IPMC actuator was analyzed, using experimental results and an analytical model. The electrical impedance and frequency response functions of the IPMC actuator were measured under four different clamping pressures. Comparing the theoretical impedance and electro-mechanical model with experimental results, it was shown that the interfacial contact resistance and torsional stiffness can be decreased and increased respectively when the clamping pressure is increased up to a certain level. The large deformation of the soft material with high clamping pressure causes a decrease in the bending performance of the IPMC actuator. We found that there is an optimum clamping pressure for getting the best actuation performance of the IPMC actuator because of a trade-off between mechanical and electrical effects. Utilizing the beam dynamics in viscous fluid with no fully clamped boundary condition, a non-homogeneous partial differential equation was developed for predicting the dynamic response of the actuator. The dynamics equation of motion has been solved by the mode superposition principle and the obtained results have been compared with experimental results. The clamping pressure should be carefully maintained and properly controlled to assure the actuation performance for practical applications of disposable IPMC actuators in biomedical devices.

Acknowledgments

This research was supported by a grant from the Fundamental R&D Program for Core Technology of Materials funded by the Ministry of Knowledge Economy, Republic of Korea (K00060282). This work was supported by a National Research Foundation of Korea grant funded by the Korean government (2010-0018423 and 2010-0000300).

References

[1] Shahinpoor M and Kim K J 2001 Ionic polymer–metal composites: I. Fundamentals *Smart Mater. Struct.* **10** 819–33
[2] Jung J H, Jeon J H, Sridhar V and Oh I K 2011 Electro-active graphene–Nafion actuators *Carbon* **49** 1279–89
[3] Guo S, Fukuda T and Asaka K 2003 A new type of fish-like underwater microrobot *IEEE/ASME Trans. Mechatronics* **8** 136–41
[4] Yeom S W and Oh I K 2009 A biomimetic jellyfish robot based on ionic polymer metal composite actuators *Smart Mater. Struct.* **18** 085002
[5] Jeon J H and Oh I K 2009 Selective growth of platinum electrodes for MDOF IPMC actuators *Thin Solid Films* **517** 5288–92
[6] Jeon J H, Kang S P, Lee S and Oh I K 2009 Novel biomimetic actuator based on SPEEK and PVDF *Sensor Actuators* B **143** 357–64
[7] Kim B, Ryu J, Jeong Y, Tak Y, Kim B and Park J 2003 A ciliary based 8-legged walking micro robot using cast IPMC actuators *Proc. IEEE Int. Conf. Robot. (Taipei)* pp 2940–5
[8] Shahinpoor M and Kim K J 2005 Ionic polymer–metal composites: IV. Industrial and medical applications *Smart Mater. Struct.* **14** 197–214
[9] Jung J H, Vadahanambi S and Oh I K 2010 Electro-active nano-composite actuator based on fullerene-reinforced Nafion *Compos. Sci. Technol.* **70** 584–92
[10] Wang X L, Oh I K and Kim J B 2009 Enhanced electromechanical performance of carbon nano-fiber reinforced sulfonated poly(styrene-*b*-[ethylene/butylene]-*b*-styrene) actuator *Compos. Sci. Technol.* **69** 2098–101
[11] Jeon J H, Yeom S W and Oh I K 2008 Fabrication and actuation of ionic polymer metal composites patterned by combining electroplating with electroless plating *Composites* A **39** 588–96
[12] McDaid A J, Aw K C, Patel K, Xie S Q and Haemmere E 2010 Development of an ionic polymer–metal composite stepper motor using a novel actuator model *Int. J. Smart Nano Mater.* **1** 261–77
[13] Wriggers P 2006 *Computational Contact Mechanics* 2nd edn (Berlin: Springer)
[14] Mishra V, Yang F and Pitchumani R 2004 Measurement and prediction of electrical contact resistance between gas diffusion layers and bipolar plate for applications to PEM fuel cells *J. Fuel Cell Sci. Technol.* **1** 2–9
[15] Zhou P, Wu C and Ma G 2007 Influence of clamping pressure on the performance of PEMFCs *J. Power Sources* **163** 874–81
[16] Lai X *et al* 2008 A mechanical–electrical finite element method model for predicting contact resistance between bipolar plate and gas diffusion layer in PEM fuel cells *J. Power Sources* **182** 153–9
[17] Wu Z *et al* 2009 An analytical model and parametric study of electrical contact resistance in proton exchange membrane fuel cells *J. Power Sources* **189** 1066–73
[18] Kanno R, Kurata A, Hattori M, Tadokoro S, Takamori T and Oguro K 1994 Characteristics and modeling of ICPF actuator *Proc. JSME Ann. Conf. Robot. Mech. (Kobe)* pp 1206–9
[19] Newbury K M and Leo D J 2003 Linear electromechanical model of ionic polymer transducers-part I: model development *J. Intell. Mater. Syst. Struct.* **14** 333–42
[20] Bonomo C, Fortuna L, Giannone P and Graziani S 2007 A nonlinear model for ionic polymer metal composites as actuators *Smart Mater. Struct.* **16** 1–12
[21] Porfiri M 2009 An electromechanical model for sensing and actuation of ionic polymer metal composites *Smart Mater. Struct.* **18** 015016
[22] Pugal D, Kim K J and Aabloo A 2011 An explicit physics-based model of ionic polymer–metal composite actuators *J. Appl. Phys.* **110** 084904
[23] Chen Z and Tan X 2008 A control-oriented and physics-based model for ionic polymer–metal composite actuators *IEEE/ASME Trans. Mechatronics* **13** 519–29
[24] Nemat-Nasser S and Li J Y 2000 Electromechanical response of ionic polymer–metal composites *J. Appl. Phys.* **87** 3321–31
[25] Farinholt K M 2005 Modeling and characterization of ionic polymer transducers for sensing and actuation *PhD Thesis* Virginia Polytechnic Institute and State University
[26] Chen Z, Shatara S and Tan X 2010 Modeling of biomimetic robotic fish propelled by an ionic polymer–metal composite caudal fin *IEEE/ASME Trans. Mechatronics* **15** 448–59
[27] Yim W, Lee J and Kim K J 2007 An artificial muscle actuator for biomimetic underwater propulsors *Bioinspr. Biomim.* **2** S31–41
[28] Nemat-Nasser S and Wu Y 2003 Comparative experimental study of ionic polymer–metal composites with different backbone ionomers and in various cation forms *J. Appl. Phys.* **93** 5255–67
[29] Vahabi M, Mehdizadeh E, Kabganian M and Barazandeh F 2011 Experimental identification of IPMC

actuator parameters through incorporation of linear and nonlinear least squares methods *Sensor Actuators* A **168** 140–8
[30] Shahinpoor M and Kim K J 2000 The effect of surface-electrode resistance on the performance of ionic polymer–metal composite (IPMC) artificial muscles *Smart Mater. Struct.* **9** 543–51
[31] Punning A, Johanson U, Anton M, Aabloo A and Kruusmaa M 2009 A distributed model of ionomeric polymer metal composite *J. Intell. Mater. Syst. Struct.* **20** 1711–24
[32] Bao X, Bar-Cohen Y and Lih S-S 2002 Measurements and macro models of ionomeric polymer–metal composites (IPMC) *Proc. SPIE-EAPAD Conf.* pp 4695–27
[33] Magrab E 2012 *Vibrations of Elastic Systems: With Applications to MEMS and NEMS* vol 184 (Berlin: Springer)
[34] Meirovitch L 1986 *Elements of Vibration Analysis* 2nd edn (New York: McGraw-Hill)
[35] Shahinpoor M and Kim K J 2001 Ionic polymer–metal composites: I. Fundamentals *Smart Mater. Struct.* **10** 819–33
[36] Zhou P, Wu C and Ma G 2006 Contact resistance prediction and structure optimization of bipolar plates *J. Power Sources* **159** 1115–22
[37] Costa Branco P J and Dente J A 2006 Derivation of a continuum model and its electric equivalent-circuit representation for ionic polymer–metal composite (IPMC) electromechanics *Smart Mater. Struct.* **15** 378–92
[38] Feng G-H and Tsai M-Y 2011 Micromachined optical fiber enclosed 4-electrode IPMC actuator with multidirectional control ability for biomedical applications *Biomed. Microdevices* **13** 169–77
[39] Yousef H, Boukallel M and Althoefer K 2011 Tactile sensing for dexterous in-hand manipulation in robotics—a review *Sensor Actuators* A **167** 171–87
[40] Santos J, Lopes B and Costa Branco P J 2010 Ionic polymer–metal composite material as a diaphragm for micropump devices *Sensor Actuators* A **161** 225–33
[41] Tiwari R and Garcia E 2011 The state of understanding of ionic polymer metal composite architecture: a review *Smart Mater. Struct.* **20** 083001
[42] Chen X, Zhu G, Yang X, Hung D L S and Tan X 2012 Model-based estimation of flow characteristics using an ionic polymer–metal composite beam *IEEE/ASME Trans. Mechatronics* in press
[43] Nakamura T, Ihara T, Horiuchi T, Mukai T and Asaka K 2009 Measurement and modeling of electro-chemical properties of ion polymer metal composite by complex impedance analysis *J. Control Meas. Syst. Integr.* **2** 373–8
[44] Bonomo C, Fortuna L, Giannone P, Graziani S and Strazzeri S 2008 A model of ionic polymer–metal composites actuators in underwater operations *Smart Mater. Struct.* **17** 025029